

**Antituberculosis drug isoniazid degraded by electro-Fenton
and photoelectro-Fenton processes using a boron-doped
diamond anode and a carbon-PTFE air-diffusion cathode**

Diego R. V. Guelfi¹, Fábio Gozzi¹, Ignasi Sirés^{2*}, Enric Brillas², Amílcar
Machulek Junior¹, Silvio César de Oliveira^{1*}

¹*Instituto de Química (INQUI), Universidade Federal de Mato Grosso do Sul, Av.
Senador Filinto Muller, 1555, Caixa postal 549, MS 79070-900 Campo Grande, Brazil*

²*Laboratori d'Electroquímica dels Materials i del Medi Ambient, Departament de
Química Física, Facultat de Química, Universitat de Barcelona, c/ Martí i Franquès 1-
11, 08028 Barcelona, Spain*

*Corresponding Author:

Tel.: +55 6733453551; Fax: +55 6733453552

E-mail address: scolive@gmail.com (S.C. de Oliveira)

E-mail address: i.sires@ub.edu (Ignasi Sirés)

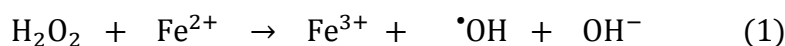
Abstract Solutions with 0.65 mM of the antituberculosis drug isoniazid (INH) in 0.050 M Na₂SO₄ at pH 3.0 were treated by electro-Fenton (EF) and UVA photoelectro-Fenton (PEF) processes using a cell with a BDD anode and a carbon-PTFE air-diffusion cathode. The influence of current density on degradation, mineralization rate and current efficiency has been thoroughly evaluated by EF. The effect of the metallic catalyst (Fe²⁺ or Fe³⁺) and the formation of products like short-chain linear aliphatic carboxylic acids were assessed by PEF. Two consecutive pseudo-first-order kinetic regions were found using Fe²⁺ as catalyst. In the first region, at short time, the drug was rapidly oxidized by •OH, whereas in the second region, at longer time, a resulting Fe(III)-INH complex was much more slowly removed by oxidants. INH disappeared completely at 300 min by EF, attaining 88% and 94% mineralization at 66.6 and 100 mA cm⁻², respectively. Isonicotinamide and its hydroxylated derivative were identified as aromatic products of INH by GC-MS and oxalic, oxamic and formic acids were quantified by ion-exclusion HPLC. The PEF treatment of a real wastewater polluted with the drug led to slower INH and TOC abatements because of the parallel destruction of its natural organic matter content.

Keywords: Electro-Fenton; Isoniazid; Oxidation products; Photoelectro-Fenton; Real wastewater; Water treatment

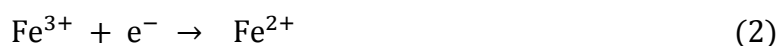
Introduction

The power and effectiveness of the electro-Fenton (EF) process regarding the mineralization of several classes of water organic pollutants make it an excellent alternative for ameliorating the existing water treatment systems. EF can be combined with conventional physicochemical and biological methods, giving rise to eco-friendly and easy-to-implement technologies (Brillas et al. 2009; Nidheesh and Gandhimathi 2012; Sirés and Brillas 2012; Martínez-Huitle et al. 2015).

In EF, the catalytic decomposition of H_2O_2 by Fe^{2+} ion according to the classical Fenton's reaction (1) promotes a large and quick production of hydroxyl radical ($\bullet\text{OH}$, $E^\circ = 2.8 \text{ V/SHE}$). This species attacks in non-selective mode the organic molecules contained in the medium with high rate constants, transforming them into more innocuous products (Brillas et al. 2009; Sirés and Brillas 2012).

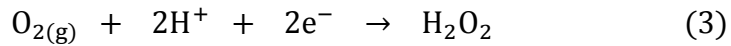


In this process, the Fe^{2+} ion is regenerated from Fe^{3+} owing to its cathodic reduction following reaction (2). This ensures the formation of $\bullet\text{OH}$ provided that H_2O_2 is continuously generated (Brillas et al. 2009; Sirés and Brillas 2012; Moreira et al. 2017).

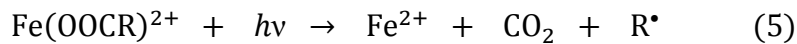
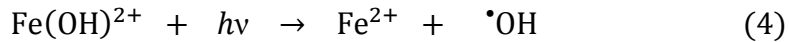


H_2O_2 is obtained by in situ electrogeneration from O_2 reduction, according to reaction (3), which is particularly favored at carbonaceous substrates (Vasudevan and Oturan 2014; Nidheesh et al. 2018). The good performance of O_2 reaction can be

ensured, for example, using hydrophobized, porous air-diffusion cathodes. Among the materials currently used for this purpose, carbon-polytetrafluoroethylene (PTFE) stands out because it presents properties such as mechanical, thermal and chemical resistance in acidic and alkaline media, along with a high catalytic ability to produce H₂O₂ (Brillas et al. 2000; Galia et al. 2016; Pérez et al. 2017).



The performance of the EF process can be improved with the use of UVA radiation (315-400 nm), which is typical in photoelectro-Fenton (PEF) since it promotes: (i) the photoreduction reaction (4) from Fe(III) species formed by Fenton's reaction (1), and (ii) the photodecomposition of Fe(III)-carboxylate complexes from reaction (5) (Brillas et al. 2009; Aguilar et al. 2017; Moreira et al. 2017).



Boron-doped diamond (BDD) anodes are preferred to upgrade the EF and PEF processes. These electrodes favor the oxidation of the water molecule, yielding poorly physisorbed BDD($\bullet\text{OH}$) on their surface by reaction (6), which in turn can attack organic molecules in competition with $\bullet\text{OH}$ formed in the bulk upon maximization of mass transport toward the BDD surface (Kapałka et al. 2008, 2009; Brillas et al. 2009; Gozzi et al. 2012; Labiadh et al., 2016).



Chemical resistance and, above all, inertness (i.e., low adsorption of molecules that result in anode fouling) of the surface are other positive characteristics of BDD as an anode for the removal of organic pollutants from water (Brillas et al. 2009; Panizza and Cerisola 2009; Sirés and Brillas 2012).

Among the various organic pollutants, pharmaceuticals have received great attention owing to their potential bioactivity (Kümmerer 2009; Martín et al. 2012; Sirés and Brillas 2012; Moreira et al. 2017). The main routes of entry of these compounds into the environment are uncontrolled discharge events from the pharmaceutical industry, hospitals and households (Verlicchi et al. 2012a, b; Barhoumi et al. 2015). Their ineffective removal in current wastewater treatment facilities causes the presence at micrograms per liter level in different water matrices (Kümmerer 2009; Verlicchi et al. 2012a, b; Brillas and Sirés 2015).

Isoniazid (INH, $C_6H_7N_3O$, isonicotinic acid hydrazide) is a widely used antibiotic against tuberculosis, a disease that affects at least a third of the world's population (Scior et al. 2002) as well bovine herds (Leite et al. 2000). As occurs with many other drugs, up to 75% of the parent compound can be excreted unchanged from the body (Sasu et al. 2015), being able to enter into water bodies. An issue that suggests a need for closer attention to the INH residues is its ability to cause bacterial resistance, as confirmed for the strain *Mycobacterium tuberculosis* (Scior et al. 2002; Kümmerer 2009), also being considered as biorefractory (Sasu et al. 2015). Only few works have reported the degradation of INH by advanced oxidation processes like photocatalysis (Guevara-Almaraz et al. 2015; Jo and Natarajan 2015a, b; Stets et al. 2018), as well as homogeneous and heterogeneous UVA photo-Fenton (Stets et al. 2018). However, no previous work about the INH removal from wastewater by electrochemical technologies has been reported in the literature.

This paper aims to assess the degradation of the antituberculosis dyes INH by EF at different applied current densities (j) and PEF with Fe^{2+} or Fe^{3+} as catalyst using a BDD/air-diffusion cell. By-products evolution was monitored by gas chromatography-mass spectrometry (GC-MS) and high performance liquid chromatography (HPLC). The trials were mainly performed in ultrapure water and compared with real wastewater matrix.

Experimental details

Chemicals

Isoniazid (analytical standard, $\geq 99\%$ purity) was purchased from Sigma-Aldrich. Analytical grade Na_2SO_4 , $\text{FeSO}_4 \cdot 7\text{H}_2\text{O}$ and $\text{Fe}(\text{NO}_3)_3 \cdot 9\text{H}_2\text{O}$ were supplied by Vetec Quimica Fina and Probus, respectively. HPLC grade acetonitrile and other analytical grade chemicals used for analysis, as well as analytical grade H_2SO_4 added to adjust the initial pH to 3.0, were purchased from Vetec Quimica Fina and Panreac. High-purity water (Millipore Milli-Q, resistivity $>18.2 \text{ M}\Omega \text{ cm}$) was used to prepare all solutions.

Real wastewater

The real wastewater corresponds to a secondary effluent of a wastewater plant facility located in Gavà-Viladecans (Barcelona, Spain) that treats urban and selected industrial wastewater. The sample had a translucent yellowish color, with particles in suspension, $\text{pH} = 7.3$ and conductivity = 1.9 mS cm^{-1} . After adjusting the pH to 3, the total organic carbon (TOC) was of 20.46 mg L^{-1} and the concentrations of anions increased as NO_3^- (0.85 mg L^{-1}) $<$ SO_4^{2-} (141.3 mg L^{-1}) $<$ Cl^- (318 mg L^{-1}), whereas that of cations as Fe^{2+}

$(0.19 \text{ mg L}^{-1}) < \text{K}^+ (4 \text{ mg L}^{-1}) < \text{Mg}^{2+} (24 \text{ mg L}^{-1}) < \text{NH}_4^+ (36.9 \text{ mg L}^{-1}) < \text{Ca}^{2+} (86 \text{ mg L}^{-1}) < \text{Na}^+ (212 \text{ mg L}^{-1})$.

Electrolytic system

EF and PEF measurements were performed in an open, undivided electrochemical cell with capacity of 150 mL and jacketed for water recirculation at 25 °C. The anode was a BDD thin-film electrode supplied by NeoCoat and the cathode was a carbon-PTFE air-diffusion electrode supplied by E-TEK. The cathode was mounted as described in earlier work (Bañuelos et al. 2016). Compressed air at 1 L min⁻¹ was pumped through its inner and dry face for continuous production of H₂O₂, whereas its outer face was in contact with the solution. Both electrodes, of 3 cm² geometric area, were separated 1 cm. All the experiments were conducted at constant j supplied by an Instrutherm Fa-3003 or an Agilent N5765A DC power supply, and the treated solutions were vigorously stirred using a magnetic bar at 800 rpm. Solutions of 100 mL with 0.65 mM INH and 0.050 M Na₂SO₄ were comparatively degraded by EF process using 0.50 mM Fe²⁺ as catalyst. For the comparative PEF treatment with UVA light, a 6 W-Satellite F6T5BLB black light tube lamp was positioned horizontally at 5 cm from the surface of the solution between the two electrodes. The UV intensity of the lamp was 5 W m⁻², as determined by a Kipp&Zonen CUV 5 radiometer. The effect of 0.50 mM Fe³⁺ as catalyst was also examined.

Instruments and analytical procedures

The pH of solutions was measured with a Crison 2000 or Crison GLP 22 pH meter. To determine the INH concentration in samples collected, they were immediately diluted with the same volume of acetonitrile to stop the degradation.

The concentration was measured by reversed-phase HPLC using a Thermo Scientific Finnigan Surveyor liquid chromatograph coupled to a photodiode array detector set at $\lambda = 215$ nm. Aliquots of 25 μL were injected into the liquid chromatograph upon elution with a (50:50) acetonitrile/water mixture at a flow rate of 0.6 mL min^{-1} , circulating through an Agilent Technologies Zorbax Eclipse XDB-C-18 5 μm , 250 $\text{mm} \times 4.6$ mm, column. The peak of INH appeared at 9.5 min, having a limit of detection (LOD) = 1.31×10^{-5} mM and limit of quantification (LOQ) = 4.58×10^{-5} mM. Ion-exclusion HPLC was utilized to quantify the generated carboxylic acids using the same equipment and procedure reported elsewhere (Gozzi et al. 2017). A Shimadzu 1800 UV/Vis spectrophotometer was used for the quantification of NH_4^+ by indophenol method (APHA 2012). The mineralization of INH solutions was assessed by injecting 50 μL aliquots into a Shimadzu TOC-V CPN analyzer, with LOD = 0.2138 mg L^{-1} and LOQ = 0.7162 mg L^{-1} . To do this analysis, the samples collected were immediately diluted with Milli-Q water (1:3), and then filtered with Whatman PTFE 0.22 μm filters prior to analysis. About $\pm 1\%$ reproducibility was found.

All the degradation and mineralization runs were made in duplicate and their average results are reported, with a standard deviation $< 5\%$. In figures, the corresponding error bars are given.

From the INH concentration decay, the apparent rate constant (k_{app}) was obtained as the slope of the pseudo-first-order linear correlation:

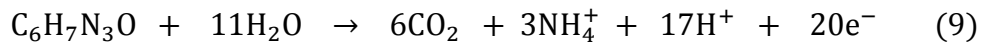
$$k_{\text{app}} = \frac{\ln\left(\frac{[\text{INH}]_0}{[\text{INH}]_t}\right)}{t} \quad (7)$$

where $[\text{INH}]_0$ and $[\text{INH}]_t$ are the initial concentration and that at time t (in min) for isoniazid, respectively.

From the experimental TOC decay ($\Delta(\text{TOC})_{\text{exp}}$, in mg L^{-1}) after time t (in h) of a given EF or PEF treatment at current I (in A), the percentage of mineralization current efficiency (MCE) was estimated as follows (Brillas et al. 2009):

$$\text{MCE}(\%) = \frac{nFV\Delta(\text{TOC})_{\text{exp}}}{4.32 \times 10^7 mIt} \times 100 \quad (8)$$

where n is the number of electrons required for total mineralization, F is the Faraday constant, V is the solution volume (in L), 4.32×10^7 is a conversion factor ($3,600 \text{ s h}^{-1} \times 12,000 \text{ mg C mol}^{-1}$) and m is the number of carbon atoms of INH (6 atoms). The n -value was taken as 20, considering the theoretical combustion reaction (9) with formation of CO_2 and NH_4^+ as the pre-eminent ion formed from the initial oxidation of N atoms:



The main and most stable INH degradation products formed during the EF treatment of 100 mL of a 1.30 mM INH solution with 0.050 M Na_2SO_4 were elucidated by GC-MS using a NIST05-MS database. The equipments and experimental conditions for this technique, using a non-polar Teknokro TR-450232 Sapiens-X5MS column, have been reported in earlier work (Guelfi et al., 2017).

The concentration of cations in the real wastewater, except NH_4^+ , was obtained

by inductively coupled plasma-optical emission spectroscopy (ICP-OES) and that of anions was determined by ion chromatography, as reported in Flores et al. (2018).

Results and discussion

Influence of current density on the EF treatment

The most important operation parameter in the EF process is the applied j , since it limits the quantity of oxidant $\bullet\text{OH}$ originated under Fenton's conditions and at the BDD surface (Sirés et al. 2014; Aguilar et al. 2017). The increase of this parameter promotes the formation of more H_2O_2 at the cathode from reaction (3), which gives rise to greater quantity of $\bullet\text{OH}$ from Fenton's reaction (1), as well as BDD($\bullet\text{OH}$) by accelerating reaction (6). Faster regeneration of Fe^{2+} from reaction (2) also occurs, additionally enhancing Fenton's reaction (1) (Sirés et al. 2014).

The influence of j between 33 and 100 mA cm^{-2} was assessed by treating a 0.65 mM (95 mg L^{-1}) INH solution with 0.50 mM Fe^{2+} as catalyst and 0.050 M Na_2SO_4 as supporting electrolyte at pH 3.0 by EF using a BDD/air-diffusion cell. The INH removal along the electrolysis is depicted in Fig. 1a. As can be seen, complete disappearance was achieved after 300 min at the lowest $j = 33.3 \text{ mA cm}^{-2}$, whereas it occurred at about 210 min operating at 66.6 and 100 mA cm^{-2} (see also Table 1). The faster INH removal up to $j = 66.6 \text{ mA cm}^{-2}$ is expected by the larger accumulation of $\bullet\text{OH}$ and BDD($\bullet\text{OH}$) from reactions (1) and (6), respectively. However, the similar INH decay when rising up to 100 mA cm^{-2} suggests the existence of parasitic reactions or the quicker formation of Fe(III) complexes that are more difficultly oxidized by the above oxidants (Guelfi et al. 2017, 2018).

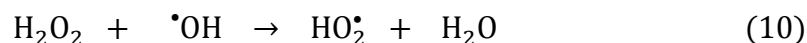
The inset panel of Fig. 1a depicts the pseudo-first-order profiles. Two consecutive kinetic regions can be distinguished. Table 1 collects the apparent rate constants for each region, $k_{app,1}$ and $k_{app,2}$, with the corresponding good R -squared (R_1^2 and R_2^2). A very fast INH concentration decay can be observed in the first region at short time, up to near 4 min, owing to the direct attack of $\bullet\text{OH}$ in the bulk onto INH and, to smaller extent, of BDD($\bullet\text{OH}$) (Gozzi et al. 2017; Guelfi et al. 2017, 2018; Moreira et al. 2017). Table 1 evidences a strong drop in the $k_{app,1}$ -value of the first region with increasing j , 0.43- and 0.18-fold lower at 66.6 and 100 mA cm⁻², respectively, compared to that found at 33.3 mA cm⁻². This phenomenon can be accounted for by the progressive formation of another electroactive species, which can be a Fe(III) complex of INH that is more rapidly generated at higher j due to the quicker Fe³⁺ production from Fenton's reaction (1). This causes a smaller oxidation of INH by $\bullet\text{OH}$ before the production of its Fe(III) complex, leading to a lower $k_{app,1}$ -value, which is in contrast to the greater production of oxidant. This behavior confirms similar results found by us for other N -aromatics (Gozzi et al. 2017; Guelfi et al. 2017, 2018).

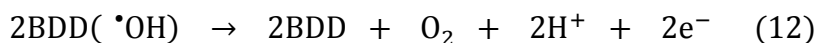
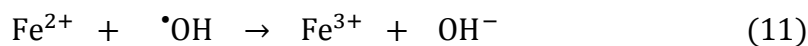
In contrast, Fig. 1a highlights that the INH concentration decayed much more slowly in the second kinetic region, observed at times from 5 to 30 min. The $k_{app,2}$ -value was almost doubled when j changed from 33.3 to 66.6 mA cm⁻², with no further enhancement. This suggests that the Fe(III)-INH complex is pre-eminently oxidized by BDD($\bullet\text{OH}$), since it has superior oxidation ability to remove Fe(III) species as compared to $\bullet\text{OH}$ (Martínez-Huitle et al. 2015). The fact that the $k_{app,2}$ -value did not increase at $j > 66.6$ mA cm⁻² indicates that additional BDD($\bullet\text{OH}$) produced was not effective because it was mainly wasted in parasitic reactions.

Regarding the TOC removal of the above trials, Fig. 1b always shows a slow regular abatement with prolonging electrolysis because many intermediates are formed

and progressively destroyed. Increasing j accelerated largely the mineralization process up to $j = 66.6 \text{ mA cm}^{-2}$, leading to similar mineralization rate at $j = 100 \text{ mA cm}^{-2}$. Table 1 highlights that after 540 min of EF treatment at the highest j , an almost overall mineralization with 94% TOC decay was achieved. At the end of this trial, 1.44 mM NH_4^+ was determined, meaning that the initial N was pre-eminently transformed into this cation (75.3%), as stated in reaction (9). This ion is expected to remain stable in solution under the present experimental conditions, as also observed for other N -compounds under similar degradation processes (Solano et al. 2015). Note that neither NO_3^- nor NO_2^- ions were detected by ion chromatography during this treatment. This means that the initial N not converted into NH_4^+ ion was lost as volatile nitrogenated products, presumably N_2 and N_xO_y , as proposed for other N -compounds treated by EF and PEF (Sirés et al. 2014; Gozzi et al. 2017; Guelfi et al. 2017).

The inset panel of Fig. 1b depicts a smaller MCE value at higher j , despite the greater production of oxidizing BDD($\bullet\text{OH}$) and $\bullet\text{OH}$. The average MCE values are listed in the last column of Table 1. This trend corroborates the parallel increase in rate of the parasitic non-oxidant reactions that decreases the concentration of both radicals with the consequent smaller participation in reactions with organics. These parasitic reactions involve, for example, the consumption of $\bullet\text{OH}$ by H_2O_2 and Fe^{2+} from reactions (10) and (11), respectively, and the oxidation of BDD($\bullet\text{OH}$) to O_2 gas from reaction (12) (Panizza and Cerisola 2009; Sirés et al. 2014). Reactions (13) and (14) are related to the generation of ozone and peroxodisulfate ion at the BDD surface, respectively, which compete with BDD($\bullet\text{OH}$) production (Panizza and Cerisola 2009).

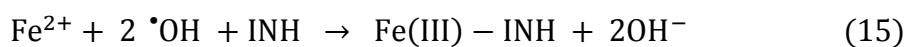




INH degradation by PEF treatment. Effect of Fe^{2+} and Fe^{3+} as catalyst

The PEF process was studied by treating a 0.65 mM INH solution in 0.050 M Na_2SO_4 with 0.50 mM Fe^{2+} or 0.50 mM Fe^{3+} as catalyst at pH 3.0 and $j = 33.3 \text{ mA cm}^{-2}$ under irradiation with a 6 W UVA lamp. Under these conditions, a very poor photolytic degradation of the drug is expected (Stets et al. 2018).

Fig. 2a illustrates that total disappearance of INH was achieved after 270 min of both PEF treatments, a time slightly shorter than 300 min required for EF under the same conditions. The slight superiority of PEF can be related to the additional oxidation of the Fe(III)-INH complex by the excess of $\bullet\text{OH}$ induced from photolytic reaction (4), in competence with the preferential attack of $\text{BDD}(\bullet\text{OH})$. This explains the quicker removal of the drug using PEF in the second kinetic region, as compared to EF (see the inset of Fig. 2a). In contrast, INH is more largely destroyed in the first kinetic region of EF, with a $k_{\text{app},1}$ -value 1.27-fold higher than that of PEF (see Table 1). This surprising behavior can be explained if $\bullet\text{OH}$ photoinduced in PEF favors a faster generation of the Fe(III)-INH complex, with a slower decay of INH in the first region, as follows:



The existence of such complex was deduced from the fact that, in PEF with 0.50 mM Fe³⁺ as catalyst, a single pseudo-first-order kinetic region was obtained (see the inset of Fig. 2a). This can be ascribed to the pre-eminent oxidation of the Fe(III)-INH complex with BDD([•]OH), since it possesses a k_{app} -value of about 0.02 min⁻¹ that is similar to the $k_{app,2}$ -values found in EF and PEF with 0.50 mM Fe²⁺ (see Table 1). Hence, the second regions obtained for the two latter processes, as well as the single region for PEF with 0.50 mM Fe³⁺, plausibly correspond to the oxidation of the same electroactive species, the Fe(III)-INH complex. This is also indicative of its photostability under UVA irradiation.

Fig. 2b shows the TOC and MCE profiles obtained for the assays of Fig. 2a. It is noticeable that the INH solution was mineralized at similar rate by PEF, regardless the catalyst added, attaining 84%-88% of TOC reduction after 540 min of electrolysis (see Table 1). It can be also observed in Fig. 2b the slower TOC decay by EF under similar conditions, with a final mineralization of 74%. The analogous mineralization rate found for both PEF processes suggests that it is limited by a similar destruction of the same products, probably corresponding to Fe(III) complexes with final short-chain linear carboxylic acids that are either photodecomposed from reaction (5) or oxidized by BDD([•]OH) (Brillas et al. 2009; Martínez-Huitle et al. 2015). Accordingly, the inset panel of Fig. 2b evidences the higher MCE values determined for PEF as compared to EF, being confirmed by the high average values for the former process given in Table 1.

Identification of primary products

Table 2 summarizes the characteristics of INH and two primary products detected by GC-MS after 5 and 30 min of EF treatment of 100 mL of 1.39 mM of the drug at $j = 33.3 \text{ mA cm}^{-2}$. These products were isonicotinamide found at 5 min and its

hydroxylated derivative identified at 30 min. Note that isonicotinamide has been previously reported as a product of INH when it was treated by TiO₂ photocatalysis with UV radiation (Guevara-Almaraz et al. 2015). To corroborate if this product can also be formed from the photolysis of the parent molecule, some assays were made by illuminating 200 mL of 2.78 mM INH in a 0.050 M Na₂SO₄ solution at pH 3.0 with a potent lamp of 160 W. After 300 min, isonicotinamide was also identified by GC-MS, meaning that INH can be very slowly photolyzed by UVA light.

It is expected that the subsequent oxidation of products causes the cleavage of the pyridine ring originating short-chain linear carboxylic acids that are mainly present in the medium as Fe(III) species (Martínez-Huitle et al. 2014; Moreira et al. 2017). Oxalic, oxamic and formic acids were identified and quantified during the PEF treatments, with 0.50 mM Fe²⁺ or 0.50 mM Fe³⁺, of a 0.65 mM INH solution at pH 3.0 and $j = 33.3 \text{ mA cm}^{-2}$. These three acids are final products since they are directly mineralized to CO₂ (Brillas et al. 2009). Fig. 3a and b illustrates the similar time course of these carboxylic acids for the two solutions tested. The main acid was formic, rapidly accumulated up to 25-28 mg L⁻¹ in only 60 min to rapidly disappear in 120-180 min, indicating a rapid photolysis of Fe(III)-formate complexes by UVA light. In contrast, oxalic and oxamic acids were accumulated to much lesser extent, and persisted largely until 300-360 min, despite the well known rapid photodecarboxylation of Fe(III)-oxalate species under UVA illumination (Brillas et al. 2009). This points to a more large production and accumulation of Fe(III)-oxalate and Fe(III)-oxamate species that are continuously oxidized with BDD(•OH) or photolyzed by UVA radiation.

The inset panels of Fig. 3a and b depict a balance of the TOC coming from all carboxylic acids, INH and their sum, compared with TOC present in solution. As can be seen, the TOC related to carboxylic acids and INH tends to zero at long electrolysis time

due to the progress of mineralization, whereas it is always much lower than that experimentally determined. This indicates the presence of a large proportion of other undetected and more recalcitrant products that explain the slow mineralization process not only by PEF, but also by EF of the INH solutions.

Based on the aforementioned results, the route of Fig. 4 is proposed for the INH mineralization by EF and PEF. The main oxidant is expressed as $\bullet\text{OH}$, denoting BDD($\bullet\text{OH}$) formed at the anode surface and/or $\bullet\text{OH}$ generated in the bulk. The process is initiated by the conversion of the parent molecule to isonicotinamide with loss of NH_4^+ ion, which can take place: (i) very slowly by photolysis with UVA light, (ii) directly by the attack of $\bullet\text{OH}$ onto INH, and (iii) the formation of the Fe(III)-INH complex, followed by its oxidation with BDD($\bullet\text{OH}$). Further attack of $\bullet\text{OH}$ over isonicotinamide causes its hydroxylation, with generation of pyridine-4-carboxamide hydroxylated. The cleavage of the pyridine ring yields a mixture of carboxylic acids such as oxalic, oxamic and formic. These acids can be either mineralized by BDD($\bullet\text{OH}$) or form Fe(III)-carboxylated complexes that are photodecomposed by UVA light with Fe^{2+} regeneration from reaction (5) or directly oxidized by BDD($\bullet\text{OH}$). The pre-eminent formation of NH_4^+ during mineralization is remarked as final product along with CO_2 .

PEF treatment in a real wastewater matrix

The study of the PEF process was extended to a real wastewater adjusted to pH 3.0, in which 0.65 mM INH was spiked along with 0.50 mM of Fe^{2+} . This solution was treated in a BDD/air-diffusion cell under UVA light (6 W lamp) at $j = 33.3 \text{ mA cm}^{-2}$. The initial TOC of the resulting solution was 70.5 mg L^{-1} , the sum of 50 mg L^{-1} from INH and 20.5 mg L^{-1} from the real wastewater, which is due to the presence of natural organic matter (NOM) that includes humic and fulvic acids.

Fig 5a shows the decay in INH concentration for the above assay compared to that obtained with the same INH concentration in 0.050 M Na₂SO₄. While in the latter conditions all the drug disappeared in 270 min, only about 70% of its concentration was reduced at 300 min. This behavior can be accounted for by the parallel attack of oxidizing agents onto NOM, diminishing the amount of them that can attack the INH molecule. Moreover, humic and fulvic acids can form complexes with Fe(II) and Fe(III) (Pullin and Cabaniss 2003), which causes a lower production of •OH from Fenton's reaction (1). Note that the high Cl⁻ concentration of the wastewater (318 mg L⁻¹) can lead to formation of active chlorine species (Cl₂/HClO) from Cl⁻ oxidation at the anode, which can attack organics competitively with BDD(•OH) and •OH (Aguilar et al. 2017; Flores et al. 2018).

The inset of Fig. 5a reveals a slower drug decay in the first region in the real wastewater, with a $k_{app,1}$ -value 0.59-fold lower than in 0.050 M Na₂SO₄ (see Table 1). This can be explained by a quicker formation of the Fe(III)-INH complex, probably due to the quicker production of Fe³⁺ from reaction (1) originated by the more rapid attack of •OH on NOM. This phenomenon is even more evident for the very slow decay found in the second region, with a 6-fold decrease of $k_{app,2}$ (see Table 1), as expected by a low oxidation of the complex by BDD(•OH) since this radical attacks pre-eminently the NOM content.

Fig. 5b shows that the normalized TOC of the real wastewater matrix containing 0.65 mM INH also decays more slowly as compared to 0.050 M Na₂SO₄, being reduced by 76% at 540 min. However, the inset of this figure evidences that greater MCE values were determined in the real wastewater matrix due to its higher TOC content, also reflected in the superior average value of 9.6% listed in the last column of Table 1. It should be noted that in the real wastewater matrix, TOC was rapidly reduced during the

first 60 min of PEF treatment, whereupon it was slightly inhibited. This can be due to the generation of recalcitrant chloroderivatives that are more slowly destroyed with the consequent loss of oxidation power of the electrolytic system.

Additional assays were made under more realistic conditions by treating a small concentration of $130 \mu\text{g L}^{-1}$ of INH by EF in both matrices. In $0.050 \text{ M Na}_2\text{SO}_4$ at pH 3.0, the drug disappeared very rapidly, needing less than 2 min at $j = 33.3 \text{ mA cm}^{-2}$ and near 7 min at $j = 3.3 \text{ mA cm}^{-2}$. This demonstrates the high oxidation power of the hydroxyl radicals originated in the BDD/air-diffusion cell to destroy INH. When the real wastewater was spiked with $130 \mu\text{g L}^{-1}$ of this drug, a much longer time of ca. 20 min was needed to remove the drug at $j = 3.3 \text{ mA cm}^{-2}$, as expected by the slower oxidation by generated hydroxyl radical due to their parallel attack onto NOM components. These findings show the viability of the Fenton-based processes to treat this drug in real systems.

Conclusions

The degradation of INH by EF and PEF with 0.50 mM Fe^{2+} shows the existence of two consecutive kinetic regions, at shorter and longer times, respectively. The pseudo-first-order profiles of the first region revealed a decrease in $k_{\text{app},1}$ -value with raising j , related to the oxidation of the parent drug with $\bullet\text{OH}$. In contrast, a much smaller $k_{\text{app},2}$ -value was found for the second region, with a little influence of j , ascribed to the destruction of a Fe(III)-INH complex by BDD($\bullet\text{OH}$). TOC decreased regularly, more rapidly at higher j , attaining an almost total mineralization with a maximum abatement of 94% after 540 min of electrolysis at $j = 100 \text{ mA cm}^{-2}$. Increasing j caused a drop in MCE due to the acceleration of parasitic reactions of hydroxyl radicals. PEF with 0.50

mM Fe³⁺ as catalyst yielded a single pseudo-first-order decay of the drug, confirming its complexation with Fe³⁺ ion. A similar TOC abatement was found using PEF with either 0.50 mM Fe²⁺ or 0.50 mM Fe³⁺ as catalyst, being greater than that observed in EF. This suggests that it was limited by the destruction of products or their Fe(III) complexes with BDD([•]OH) and UVA light. Two primary intermediates were identified by GC-MS, and oxalic, oxamic and formic acids were quantified by ion-exclusion HPLC. A reaction scheme involving all these products is proposed for INH mineralization. A final PEF study considering INH spiked into a real wastewater matrix revealed a slower degradation and TOC removal, but with higher MCE.

Acknowledgments

The authors thank funding from the Brazilian funding agencies: Fundação de Apoio ao Desenvolvimento do Ensino, Ciência e Tecnologia do Estado de Mato Grosso do Sul (FUNDECT-MS), Pró-Reitoria de Pesquisa e Pós-Graduação da Universidade Federal de Mato Grosso do Sul (PROPP-UFMS), Coordenação de Aperfeiçoamento de Pessoal de Nível Superior (CAPES), Conselho Nacional de Desenvolvimento Científico e Tecnológico (CNPQ). The authors also thank financial support from project CTQ2016-78616-R (AEI/FEDER, EU).

References

Aguilar ZG, Brillas E, Salazar M, Nava JL, Sirés I (2017) Evidence of Fenton-like reaction with active chlorine during the electrocatalytic oxidation of Acid Yellow 36 azo dye with Ir-Sn-Sb oxide anode in the presence of iron ion. *Appl Catal B: Environ* 206:44-52. doi: 10.1016/j.apcatb.2017.01.006

APHA (2012) Standard methods for the Examination of Water and Wastewater, 22th ed., American Public Health Association, New York.

Bañuelos JA, García-Rodríguez O, El-Ghenymy A, Rodríguez-Valadez F J, Godínez LA, Brillas E (2016) Advanced oxidation treatment of malachite green dye using a low cost carbon-felt air-diffusion cathode. *J Environ Chem Eng* 4(2):2066-2075. doi: 10.1016/j.jece.2016.03.012

Barhoumi N, Labiadh L, Oturan MA, Oturan N, Gadri A, Ammara S, Brillas E (2015) Electrochemical mineralization of the antibiotic levofloxacin by electro-Fenton process. *Chemosphere* 141:250-257. doi: 10.1016/j.chemosphere.2015.08.003

Brillas E, Calpe JC, Casado J (2000) Mineralization of 2,4-D by advanced electrochemical oxidation processes. *Water Res* 34(8):2253-2262. doi: 10.1016/S0043-1354(99)00396-6

Brillas E, Sirés I (2015) Electrochemical removal of pharmaceuticals from water streams: reactivity elucidation by mass spectrometry. *TrAC-Trends Anal Chem* 70:112-121. doi: 10.1016/j.trac.2015.01.013

Brillas E, Sirés I, Oturan MA (2009) Electro-Fenton process and related electrochemical technologies based on Fenton's reaction chemistry. *Chem Rev* 109:6570-6631. doi: 10.1021/cr900136g

Flores N, Brillas E, Centellas F, Rodríguez RM, Cabot PL, Garrido JA, Sirés I (2018) Treatment of olive oil mill wastewater by single electrocoagulation with different electrodes and sequential electrocoagulation/electrochemical Fenton-based processes. *J Hazard Mater* 347:58-66. doi: 10.1016/j.jhazmat.2017.12.059

Galia A, Lanzalaco S, Sabatino MA, Dispenza C, Scialdone O, Sirés I (2016) Crosslinking of poly(vinylpyrrolidone) activated by electrogenerated hydroxyl

- radicals: A first step towards a simple and cheap synthetic route of nanogel vectors. *Electrochem Commun* 62:64-68. doi: 10.1016/j.elecom.2015.12.005
- Gozzi F, Sirés I, Thiam A, Oliveira SC, Machulek Jr A, Brillas E (2017) Treatment of single and mixed pesticide formulations by solar photoelectro-Fenton using a flow plant. *Chem Eng J* 310:503-513. doi: 10.1016/j.cej.2016.02.026
- Guelfi DRV, Gozzi F, Sirés I, Brillas E, Machulek Jr A, de Oliveira SC (2017) Degradation of the insecticide propoxur by electrochemical advanced oxidation processes using a boron-doped diamond/air-diffusion cell, *Environ Sci Pollut Res* 24:6083-6095. doi: 10.1007/s11356-016-6416-8
- Guelfi, DRV, Gozzi F, Machulek Jr A, Sirés I, Brillas E, de Oliveira, SC (2018). Degradation of herbicide S-metolachlor by electrochemical AOPs using a boron-doped diamond anode. *Catal Today*. doi: 10.1016/j.cattod.2017.10.026
- Guevara-Almaraz E, Hinojosa-Reyes L, Caballero-Quintero A, Ruiz-Ruiz E, Hernández-Ramírez A, Guzman-Mar JL (2015) Potential of multisyringe chromatography for the on-line monitoring of the photocatalytic degradation of antituberculosis drugs in aqueous solution. *Chemosphere* 121:68-75. doi: 10.1016/j.chemosphere.2014.11.012
- Jo WK, Natarajan TS (2015a) Facile synthesis of novel redox-mediator-free direct Z-scheme CaIn_2S_4 Marigold-Flower-like/ TiO_2 photocatalysts with superior photocatalytic efficiency. *ACS Appl Mater Interfaces* 7:17138-17154. doi: 10.1021/acsami.5b03935
- Jo WK, Natarajan TS (2015b) Influence of TiO_2 morphology on the photocatalytic efficiency of direct Z-scheme $\text{g-C}_3\text{N}_4/\text{TiO}_2$ photocatalysts for isoniazid degradation. *Chem Eng J* 281:549-565. doi: 10.1016/j.cej.2015.06.120

- Kapałka A, Fóti G, Comninellis C (2009) The importance of electrode material in environmental electrochemistry formation and reactivity of free hydroxyl radicals on boron-doped diamond electrodes. *Electrochim Acta* 54:2018-2023. doi:10.1016/j.electacta.2008.06.045
- Kapałka A, Lanova B, Baltruschat H, Fóti G, Comninellis C (2008) Electrochemically induced mineralization of organics by molecular oxygen on boron-doped diamond electrode. *Electrochem Commun* 10:1215-1218. doi:10.1016/j.elecom.2008.06.005
- Kümmerer K (2009) Antibiotics in the aquatic environment—A review. Part I. *Chemosphere* 75(4):417-434. doi: 10.1016/j.chemosphere.2008.11.086
- Labiadh L, Barbucci A, Carpanese MP, Gadri A, Panizza M (2016) Comparative depollution of Methyl Orange aqueous solutions by electrochemical incineration using TiRuSnO₂, BDD and PbO₂ as high oxidation power anodes. *J Electroanal Chem* 766:94-99. doi: 10.1016/j.jelechem.2016.01.036
- Leite RMH, Leite RC, Lima JA, Foscolo CB, Mota PMPC, Lobato FCF, Lage AP (2000) HPLC identification of isoniazid residues in bovine milk. *Arq Bras Med Vet Zootec* 52(6):662-668. doi: 10.1590/S0102-09352000000600018
- Martín J, Camacho-Muñoz D, Santos JL, Aparicio I, Alonso E (2012) Occurrence of pharmaceutical compounds in wastewater and sludge from wastewater treatment plants: removal and ecotoxicological impact of wastewater discharges and sludge disposal. *J Hazard Mater* 239-240:40-47. doi: 10.1016/j.jhazmat.2012.04.068
- Martínez-Huitle CA, Rodrigo MA, Sirés I, Scialdone O (2015) Single and coupled electrochemical processes and reactors for the abatement of organic water pollutants: a critical review. *Chem Rev* 115:13362-13407. doi: 10.1021/acs.chemrev.5b00361

- Moreira FC, Boaventura RAR, Brillas E, Vilar VJP (2017) Electrochemical advanced oxidation processes: a review on their application to synthetic and real wastewaters. *Appl Catal B: Environ* 202:217-261. doi: 10.1016/j.apcatb.2016.08.037
- Nidheesh PV, Gandhimathi R (2012) Trends in electro-Fenton process for water and wastewater treatment: an overview. *Desalination* 299:1-15. doi: 10.1016/j.desal.2012.05.011
- Nidheesh PV, Zhou M, Oturan MA (2018) An overview on the removal of synthetic dyes from water by electrochemical advanced oxidation processes. *Chemosphere* 197:210-227. doi: 10.1016/j.chemosphere.2017.12.195
- Panizza M, Cerisola G (2009) Direct and mediated anodic oxidation of organic pollutants. *Chem Rev* 109:6541-6569. doi: 10.1021/cr9001319
- Pérez JF, Sáez C, Llanos J, Cañizares P, López C, Rodrigo MA (2017) Improving the efficiency of carbon cloth for the electrogeneration of H₂O₂: role of polytetrafluoroethylene and carbon black loading. *Ind Eng Chem Res* 56(44):12588-12595. doi: 10.1021/acs.iecr.7b02563
- Pullin MJ, Cabaniss SE (2003) The effects of pH, ionic strength, and iron-fulvic acid interactions on the kinetics of non-photochemical iron transformations. II. The kinetics of thermal reduction. *Geochim Cosmochim Acta* 67(21):4079-4089. doi: 10.1016/S0016-7037(03)00367-3
- Sasu S, Metzger JW, Kranert M, Kümmerer K (2015) Biodegradation of the antituberculosis drug isoniazid in the aquatic environment. *Clean-Soil Air Water* 43(2):166-172. doi: 10.1002/clen.201100147

- Scior T, Meneses Morales I, Garcés Eisele SG, Domeyer D, Laufer S (2002). Antitubercular isoniazid and drug resistance of Mycobacterium tuberculosis-A review. *Archiv Pharm* 335(11-12):511 -525. doi: 10.1002/ardp.200290005
- Sirés I, Brillas E, Oturan MA, Rodrigo MA, Panizza M (2014) Electrochemical advanced oxidation processes: today and tomorrow. A review. *Environ Sci Pollut Res* 21(14):8336-8367. doi: 10.1007/s11356-014-2783-1
- Sirés I, Brillas E (2012) Remediation of water pollution caused by pharmaceutical residues based on electrochemical separation and degradation technologies: a review. *Environ Int* 40:212-229. doi: 10.1016/j.envint.2011.07.012
- Solano AMS, Garcia-Segura S, Martínez-Huitle CA, Brillas, E (2015) Degradation of acidic aqueous solutions of the diazo dye Congo Red by photo-assisted electrochemical processes based on Fenton's reaction chemistry. *Appl Catal B: Environ* 168-169:559-571. doi: 10.1016/j.apcatb.2015.01.019
- Stets S, do Amaral B, Schneider JT, de Barros IR, de Liz MV, Ribeiro RR, Nagata N, Peralta-Zamora P (2018). Antituberculosis drugs degradation by UV-based advanced oxidation processes. *J Photochem Photobiol A: Chem* 353:26-33. doi: 10.1016/j.jphotochem.2017.11.006
- Vasudevan S, Oturan MA (2014) Electrochemistry: as cause and cure in water pollution-an overview. *Environ, Chem. Lett.* 12(1):97-108. doi: 10.1007/s10311-013-0434-2
- Verlicchi P, Al Aukidy M, Galletti A, Petrovic M, Barceló D (2012a) Hospital effluent: investigation of the concentrations and distribution of pharmaceuticals and environmental risk assessment. *Sci Total Environ* 430:109-118. doi: 10.1016/j.scitotenv.2012.04.055

Verlicchi P, Al Aukidy M, Zambello E (2012b) Occurrence of pharmaceutical compounds in urban wastewater: Removal, mass load and environmental risk after a secondary treatment-A review. *Sci Total Environ* 429:123-155. doi: 10.1016/j.scitotenv.2012.04.028

Figure captions

Fig. 1 Degradation curves (a) and TOC decay (b) obtained for the EF treatment of 100 mL of a 0.65 mM INH (TOC 50 mg L⁻¹) solution with 0.050 M Na₂SO₄ and 0.50 mM Fe²⁺ using an open and undivided cell with a 3 cm² BDD anode and 3 cm² carbon-PTFE air-diffusion cathode at pH 3.0, 25 °C and different current densities (*j*): (□) 33.3 mA cm⁻², (●) 66.6 mA cm⁻² and (◇) 100 mA cm⁻². The inset panels depict the pseudo-first-order kinetics for INH (a) and the mineralization current efficiency (b).

Fig. 2 Degradation curves (a) and TOC decay (b) for the treatment of 100 mL of 0.65 mM INH solutions under the same conditions of Fig. 1 at *j* = 33.3 mA cm⁻² by (□) EF with 0.50 mM Fe²⁺ and PEF with a 6 W UVA lamp using (●) 0.50 mM Fe²⁺ and (△) 0.50 mM Fe³⁺. The inset panels present the corresponding pseudo-first-order reaction for INH decay (a) and the mineralization current efficiency (b).

Fig. 3 Time course of the concentration of oxalic (□), oxamic (○) and formic (△) acids during the PEF treatment shown in Fig. 2, using 0.50 mM Fe²⁺ (a) and 0.50 mM Fe³⁺ (b). The inset panels show the behavior of TOC arising from: all carboxylic acids (■), INH (●), the sum of carboxylic acids and INH (▲) and remaining TOC (◆).

Fig. 4 Scheme for the main mineralization route of INH proposed for EF and PEF treatments, where •OH denotes the hydroxyl radical formed at the BDD surface from water oxidation or in the bulk from Fenton's reaction.

Fig. 5 Degradation curves (a) and normalized TOC decay (b) obtained for the PEF treatment of 100 mL of 0.65 mM INH in 0.050 M Na₂SO₄ solution (□) or tertiary

wastewater (▲), both with 0.50 mM Fe²⁺ at $j = 33.3 \text{ mA cm}^{-2}$, 25 °C and pH ~ 3.0. The inset panels present the pseudo-first-order kinetics for INH (a) and the mineralization current efficiency (b).

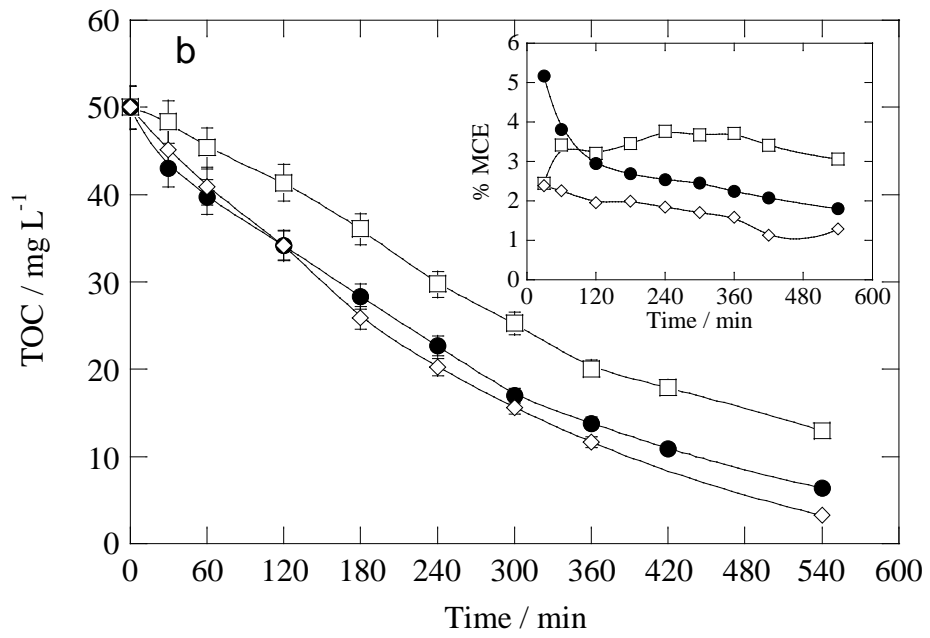
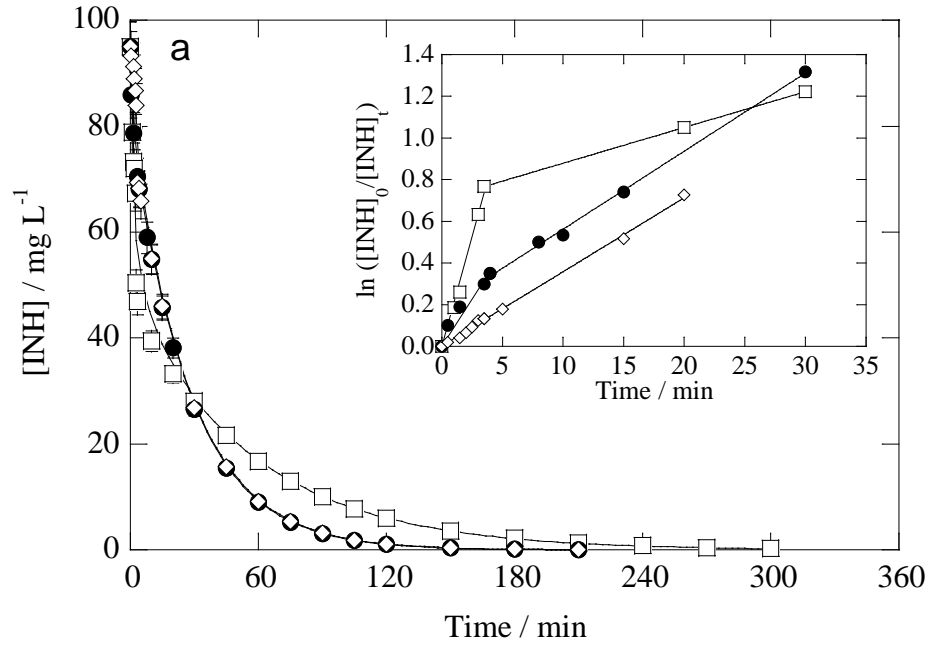


Fig. 1

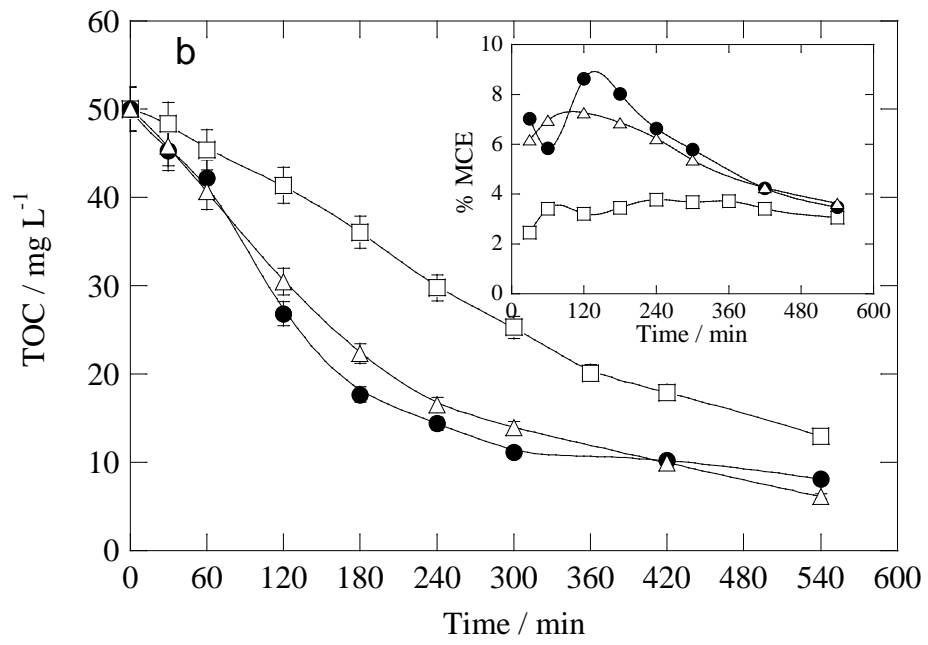
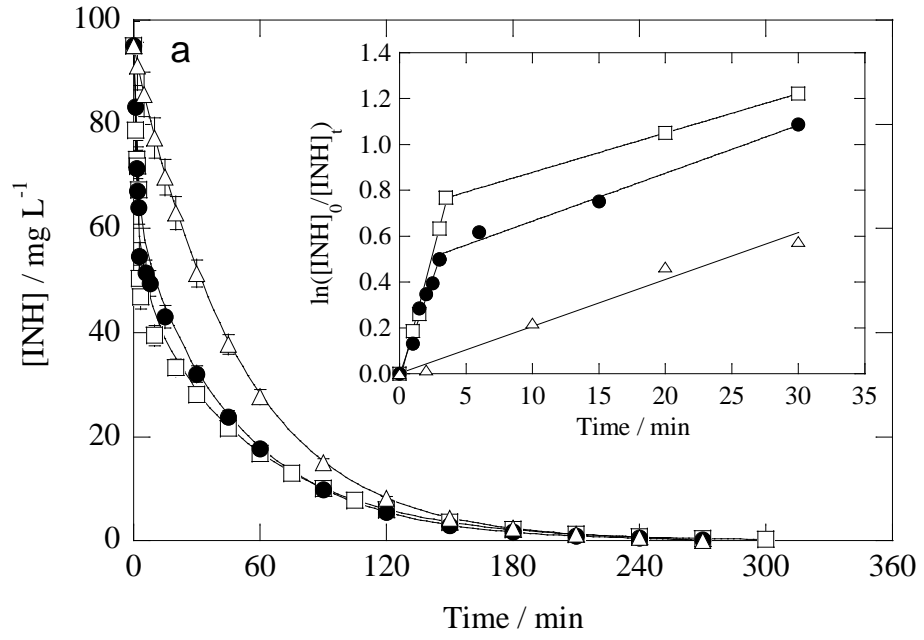


Fig. 2

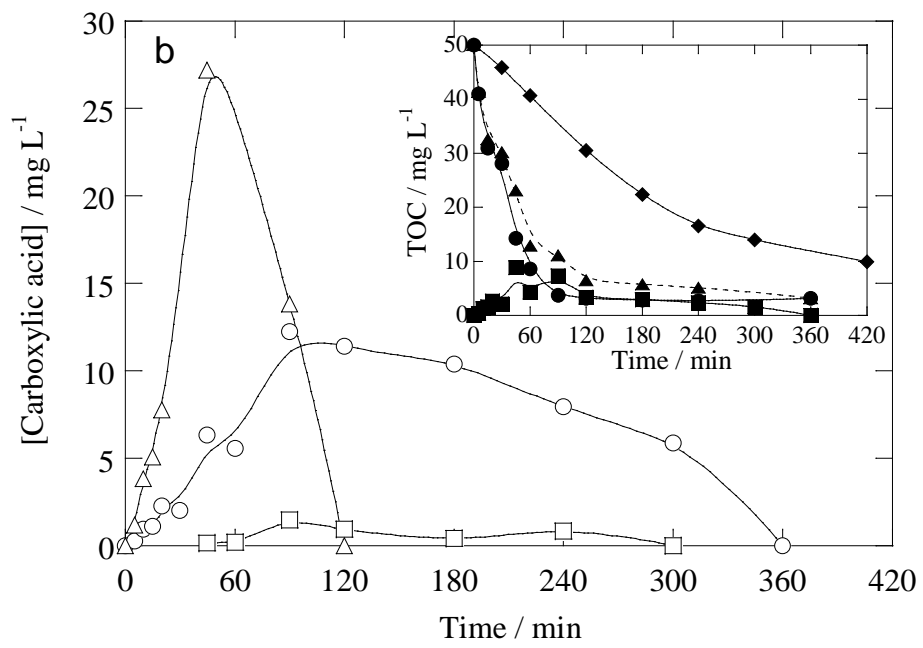
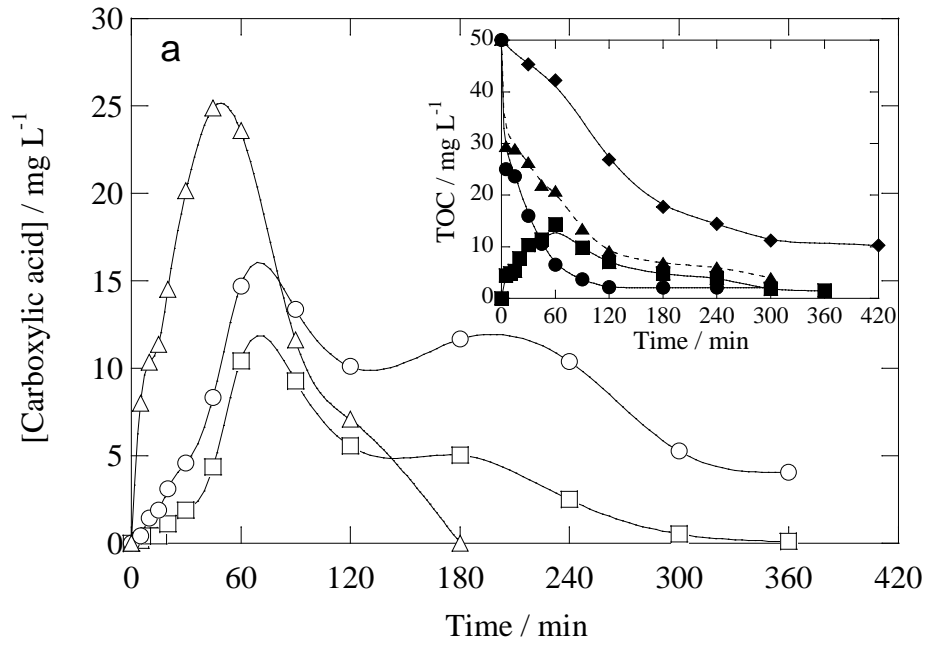


Fig. 3

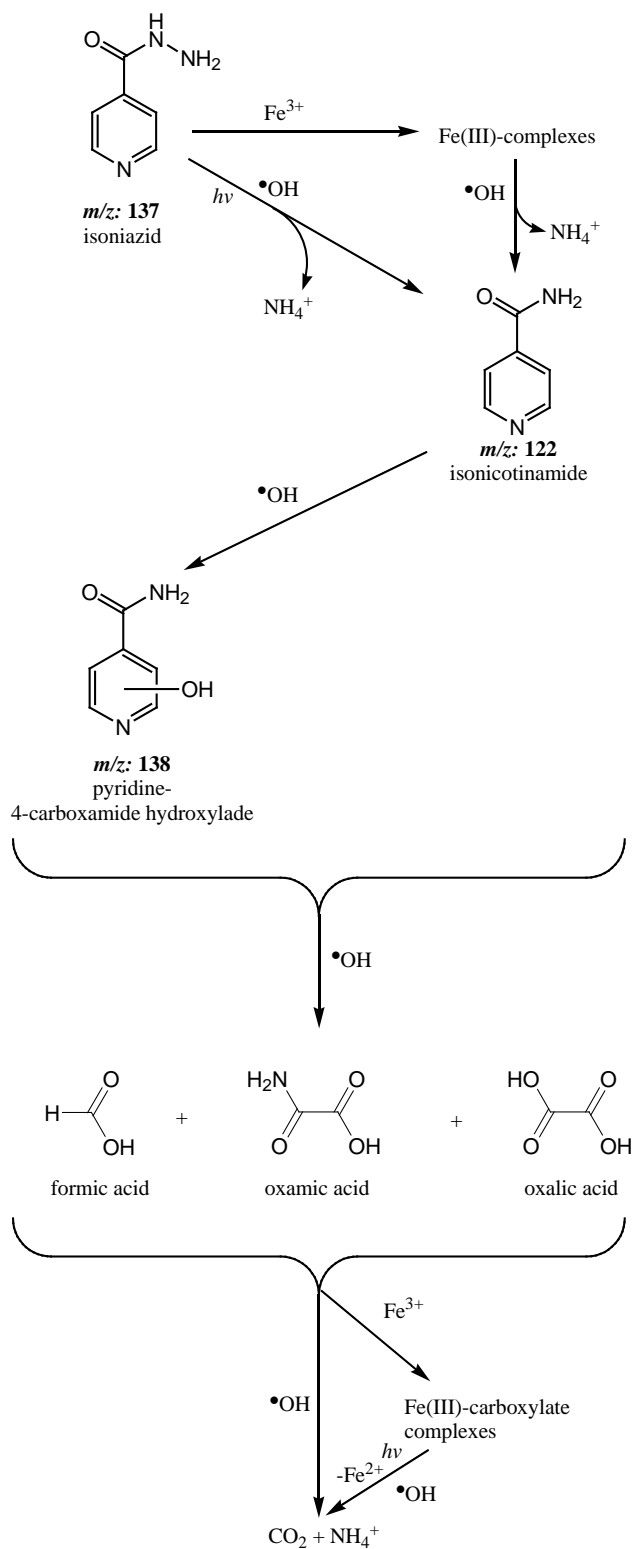


Fig. 4

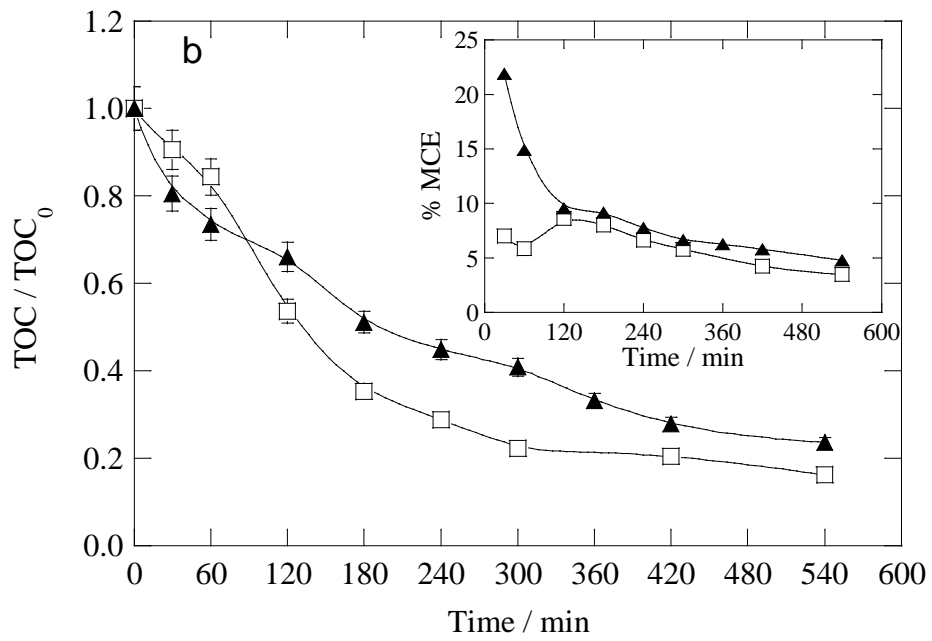
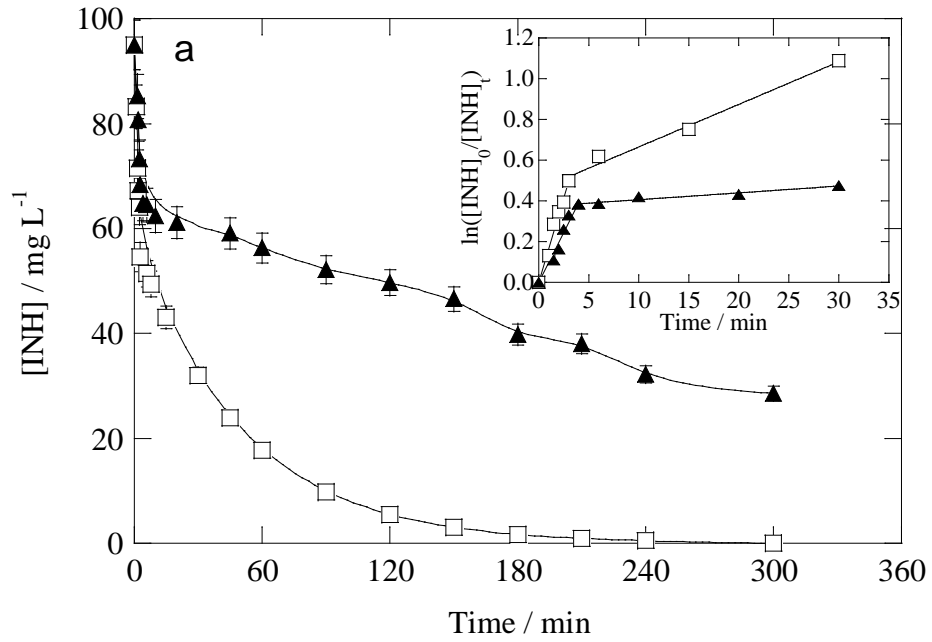


Fig. 5

Table 1 Conditions and results for the degradation of 100 mL of solutions containing isoniazid (INH) at pH 3.0 and 25 °C by EF and PEF using an open and undivided cell with a 3 cm² BDD anode and 3 cm² carbon-PTFE air-diffusion cathode.

Method	[INH] ₀ (mM)	Matrix	[Fe ²⁺] (mM)	Conductivity (mS cm ⁻¹)	<i>j</i> ^a (mA cm ⁻²)	% INH removal (<i>t</i> in min)	<i>k</i> _{app,1} ^b (min ⁻¹)	<i>R</i> ₁ ²	<i>k</i> _{app,2} ^c (min ⁻¹)	<i>R</i> ₂ ²	% TOC removal (at 540 min)	% MCE (average)
EF	0.65	0.050 M Na ₂ SO ₄	0.50	6.8	33.3	100 (300)	0.2106	0.995	0.0172	0.999	74	3.4
	0.65	0.050 M Na ₂ SO ₄	0.50	6.8	66.6	100 (210)	0.0904	0.970	0.0374	0.998	88	2.9
	0.65	0.050 M Na ₂ SO ₄	0.50	6.8	100	100 (210)	0.0375	0.982	0.0355	0.998	94	1.8
PEF	0.65	0.050 M Na ₂ SO ₄	0.50	6.8	33.3	100 (270)	0.1659	0.994	0.0209	0.989	84	6.2
	0.65	0.050 M Na ₂ SO ₄	0.50 ^d	6.8	33.3	100 (270)	0.0205	0.989	-	-	88	5.8
	0.65	RWW ^f	0.50	2.5	33.3	70 (300)	0.0986	0.978	0.0033	0.946	76	9.6

^a Current density

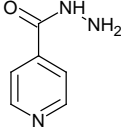
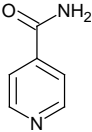
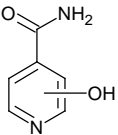
^b *k*_{app,1}: apparent rate constant of single (PEF with Fe³⁺) or first (in EF and PEF) region.

^c *k*_{app,2}: apparent rate constant of second region.

^d Fe³⁺ instead of Fe²⁺

^f RWW: real wastewater

Table 2 Products identified by GC-MS after 5 and 30 min of EF degradation of 100 mL of a 1.39 mM isoniazid solution in 0.050 M Na₂SO₄ with 0.50 mM Fe²⁺ at pH 3.0 using a stirred BDD/air-diffusion cell at 33.3 mA cm⁻², or after 300 min of photolysis of 200 mL of 2.78 mM of INH in 0.050 M Na₂SO₄ at pH 3.0 using a 160 W UVA lamp.

Compound	Molecular structure	Retention time (min)	<i>m/z</i>	Fragments (leaving group)
Isoniazid		25.5	137	106 (-NHNH ₂) 78 (=CO) 51 (=NCH)
Isonicotinamide		26.2	122	106 (-NH ₂) 78 (=CO) 51 (=NCH)
Pyridine-4-carboxamide hydroxylated		8.98	138	122 (-NH ₂ or =O) 107 (-OH and -N=, or, -OH and -NH ₂) 77 (-CONH ₂ and -OH)